J Nanopart Res (2022) 24: 183
https://doi.org/10.1007/s11051-022-05554-9

RESEARCH PAPER

Synthesis of iron oxide nanoparticles by decomposition of iron-oleate: influence of the heating rate on the particle size

Aladin Ullrich ·
Mohammad Mostafizar Rahman · Ahmed Azhar ·
Michael Kühn · Manfred Albrecht

Received: 22 January 2022 / Accepted: 10 August 2022 / Published online: 2 September 2022

Abstract Nanoparticles from transition metal oxides can be synthesized in various ways. A common synthesis route uses metal-oleate complex precursors that can be thermally decomposed, leading to crystalline metal-oxide nanoparticles with a narrow size distribution. The morphology of nanoparticles synthesized in such a way is strongly influenced by the synthesis parameters. In this study, the influence of the heating profile during the decomposition of iron oleate precursor on the size of the resulting iron oxide nanoparticles in the presence of surfactants was investigated. As surfactants oleic acid and sodium oleate were utilized for nanoparticle synthesis allowing additionally for shape control. Most of the prepared nanoparticles reveal a characteristic core–shell structure. The dominant structure is the cubic spinel structure of maghemite (γ-$(Fe^{3+})_2O_3$) or magnetite ($Fe^{2+}(Fe^{3+})_2O_4$), while in the core region of the nanoparticles, wustite ($Fe^{2+}O$) is present. The heating rate applied for the nanoparticle synthesis was systematically varied from 1 to 30 °C/min, while all other parameters were kept constant. A strong increase of the particle size (> 20 nm) was observed for low heating rates, which could be explained qualitatively in the frame of the LaMer model and allows for fine-tuning and control of the particle size.

Keywords Nanoparticles · Iron oxide nanoparticles · Iron oleate · Thermal decomposition · Heating rate

A. Ullrich (✉) · M. M. Rahman · A. Azhar · M. Kühn · M. Albrecht
Institute of Physics, University of Augsburg, Universitätsstr. 1, 86159 Augsburg, Germany
e-mail: aladin.ullrich@physik.uni-augsburg.de

M. M. Rahman
e-mail: mmostafizmst@gmail.com

A. Azhar
e-mail: azhar1992chemist@gmail.com

M. Kühn
e-mail: Michael.kuehn@student.uni-augsburg.de

M. Albrecht
e-mail: manfred.albrecht@physik.uni-augsburg.de

Motivation

Transition metal oxide nanoparticles show interesting size- and shape-dependent properties due to their wide diversity of their crystal structure and metal oxidation states. In particular, ferrite nanoparticles can be used in many different fields like sensor technology [1], spintronics [2], catalysis [3], various medical applications (hyperthermia, contrast agent, targeted drug delivery, theragnostic applications) [4–10], or water treatment [11–13].

A widely applied method for the synthesis of such nanoparticles is the thermal decomposition of metal oleate precursors in high boiling solvents such as 1-octadecene [14, 15]. A common drawback of this method is the limited size of the nanoparticles. In

most cases, the size of the particles ranges between 10 and 20 nm [14, 16–18]. Larger particles are hard to achieve by this method but might be useful for certain applications, e.g. in the field of hyperthermia [19].

In this study, however, it is demonstrated that iron oxide nanoparticles > 20 nm can be easily synthesized using different surfactants of oleic acid and sodium oleate by lowering the heating rate during the synthesis to 1 °C/min. The underlying formation process could be explained qualitatively in the frame of the LaMer model [20]. Similar behaviour has been observed [21–23] and simulated [22] by other groups for different precursor-solvent systems. Here, we demonstrate that this is also valid for the abovementioned iron-oleate precursor in 1-octadecene as solvent in combination with surfactants.

Sample preparation

Iron oxide nanoparticles were synthesized following the method of Park et al. [14]. This method is quite robust and delivers usually monodisperse particles. The size and shape of the particles depends on the synthesis parameters, particularly on the used surfactants. Typical surfactants are oleic acid or sodium oleate [17]. The corresponding metal oleate precursors were synthesized from oleic acid and the corresponding metal chloride salts.

Precursor preparation

The iron (III) oleate precursor was prepared shortly before the particle synthesis to avoid aging effects that can affect the reproducibility [24].

The iron oleate precursor was synthesized by the reaction of 10 mmol $FeCl_3 \cdot 6H_2O$ with 30 mmol oleic acid (HOl) in the presence of 30 mmol NaOH in a solvent mixture of n-hexane (18 ml), EtOH (10 ml), and water (8 ml), under nitrogen blanket. The solution was stirred by a magnetic stirrer during the whole process. The reaction mixture was heated up and kept at its boiling point of ~ 60 °C for 4 h in a three-neck flask with reflux condenser, nitrogen inlet (gas flow of approx. 1 ml/s), and thermometer.

After cooling down to room temperature (RT), the iron oleate was separated in a separation funnel and washed three times with 10 ml water. After washing, it was dried under vacuum for 5 h at ~ 50 °C, until a dark brown, highly viscous liquid was obtained.

Particle preparation

For particle synthesis, the precursor and surfactants were diluted in 1-octadecene under nitrogen atmosphere. If not stated otherwise, 10 ml of 1-octadecene and 1 g (1.11 mmol) of iron oleate were used. Different amounts of pure HOl as well as a mixture of HOl and sodium oleate (NaOl) have been used as surfactants. The 1-octadecene was degassed in advance for 30 min at ~ 50 °C under vacuum to remove oxygen. During this procedure, the flask was vented three times with dry nitrogen and evacuated again. The reaction flask was heated by a heating mantle with variable heating power. To decompose the precursor, the reaction solution was heated up to 318 °C at a controlled heating rate, ranging from 1 to 30 °C per min. The heating rate was kept linear for all heating rates except 1 °C/min. Here, the mixture was heated up to 100 °C at a higher heating rate first before the 1 °C/min rate was adjusted. Typical heating profiles that were recorded during the synthesis of the nanoparticles are shown in Fig. 1. As can be seen, the temperature profiles show a perfect linear behaviour for high heating rates, while for the 1 °C/min run there are some minor fluctuations visible.

During the decomposition, the solution was stirred by a magnetic stirrer and a continuous N_2 flow of

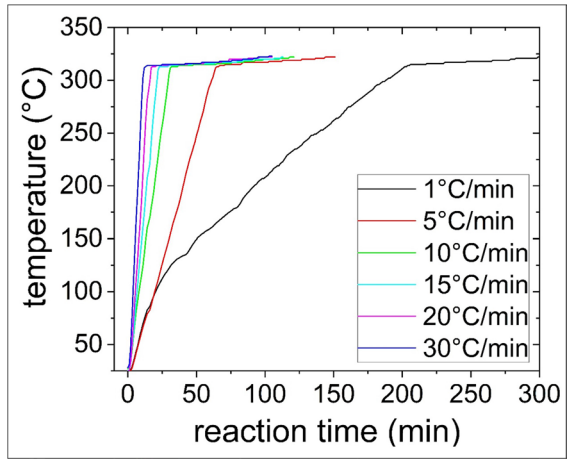

Fig. 1 Typical heating rate profiles used for the particle synthesis

approx. 1 ml/s was applied. The 1-octadecene level was kept constant by a reflux condenser.

The reaction solution was typically kept at the boiling point for 90 min. After that, the heater was switched off and the solution was allowed to cool down to RT still under nitrogen flow and stirring.

Sample preparation for TEM analysis

For transmission electron microscopy (TEM) analysis, 1 ml of the particle containing dispersion was diluted and shaken well with 2–3 ml n-hexane, and then, the particles were precipitated by adding 10–12 ml isopropanol. The dispersion was centrifuged, the clear solution poured away, and the particles were re-dispersed in 2–3 ml n-hexane. This cleaning procedure was applied three times. Finally, a carbon coated copper grid was dipped in the dispersion for 1 s. The grid was dried under ambient conditions before the TEM study was performed. For TEM analysis, a JEOL JEM F200 operated at 200 keV beam energy was used. The electron energy loss spectra (EELS) were measured with a GATAN Continuum S EELS spectrometer.

Results

Conventional bright field TEM images of the nanoparticles synthesized at different heating rates varied from 1 up to 30 °C/min and applying a mixture of NaOl (0.075 mmol/ml) and HOl (0.075 mmol/ml) as surfactants are shown in Fig. 2a–d. Clearly, nanoparticles with cubic shape and sizes from 17 to 27 nm (averaged edge length) were obtained. However, most striking, the largest sizes were achieved by using the lowest heating rate of 1 °C/min. Please note that employing a lower amount of 0.025 mmol/ml of HOl and NaOl led to nanoparticles with sizes from 17 to 28 nm without cubic morphology (not shown). As reference, runs without surfactants were performed as well. In this case, decomposing the precursor without surfactants resulted in more spherically shaped nanoparticles with sizes from 13 to 24 nm (Fig. 2e and f).

To obtain spherical particles, HOl was used as surfactant. The results for different amounts of HOl (0.025 mmol/ml and 0.63 mmol/ml) are shown in Fig. 3. Large nanoparticles from 15 to 35 nm (averaged diameter) could be prepared with a low amount

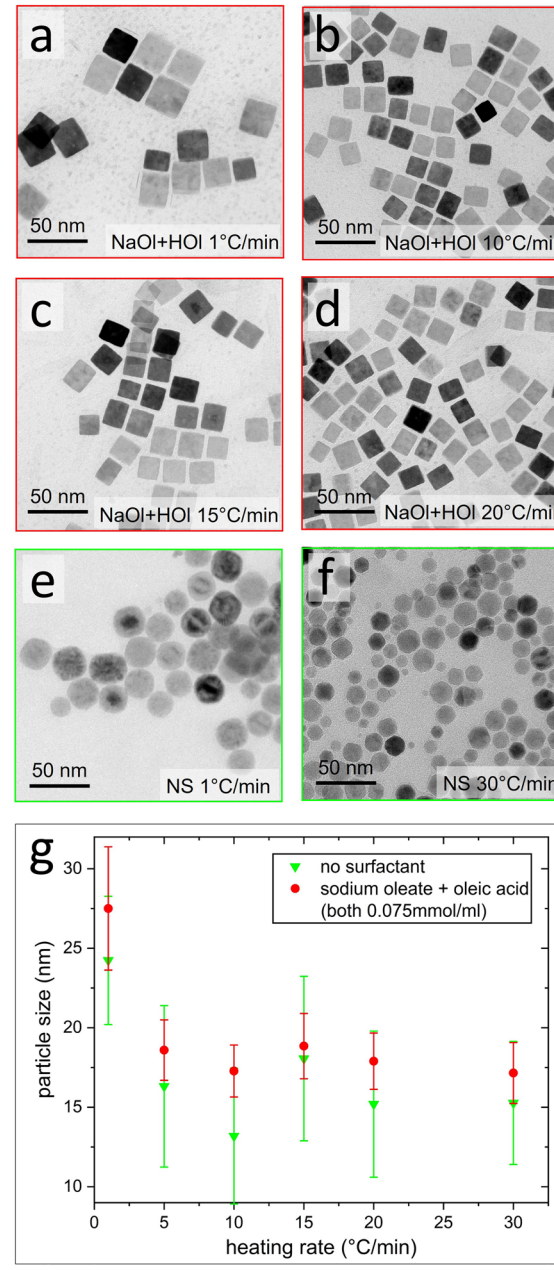

Fig. 2 TEM images of particles prepared (**a**–**d**) with NaOl/HOl mixture as surfactant and (**e**–**f**) without surfactant (NS). (**g**) Corresponding averaged particle size as a function of heating rate

(0.025 mmol/ml) of HOl (Fig. 3a and b), whereas a higher amount (0.63 mmol/ml) resulted in smaller particles (7–10 nm, Fig. 3c and d). Again, the largest spherical nanoparticles are achieved at the lowest heating rate of 1 °C/min (Fig. 3a).

The sizes of the nanoparticles for both surfactants as function of heating rate are displayed in Figs. 2g and 3e, respectively. There is a clear tendency of the average particle size to decrease with increasing heating rate for the case of HlO as surfactant (Fig. 3e). A similar behaviour is observed for the cubic particles using NaOl/HOl, but here, the nanoparticle size saturates for heating rates > 5 °C/min (Fig. 2g).

The shape control by the surfactants is consistent with the literature [16, 17]. The cubic particles are formed because of an anisotropic growth rate. This is due to the fact that the adhesion of the oleate ions is different for different crystallographic planes. Since the NaOl dissociates easier than the HOl [25] and the Ol^- ions stick to the particles surface, the shape control is stronger for the case of NaOl. The growth speed of the {100} facets is slowed down by the oleic acid ions, resulting in nanocrystals confined by these facets [17]. The dissociation of the pure HOl is less and hence there is no preferred growth direction, resulting in spherical or almost spherical shapes. As can be seen from Fig. 2a–d, most of the cubes prefer to lie down with their {100} facets to the substrate.

The size distributions of the nanoparticles are summarized in Fig. 4. The cubic particles prepared with NaOl/HOl are nearly monodisperse with a standard deviation of around 10% (Fig. 4a). Using HOl,

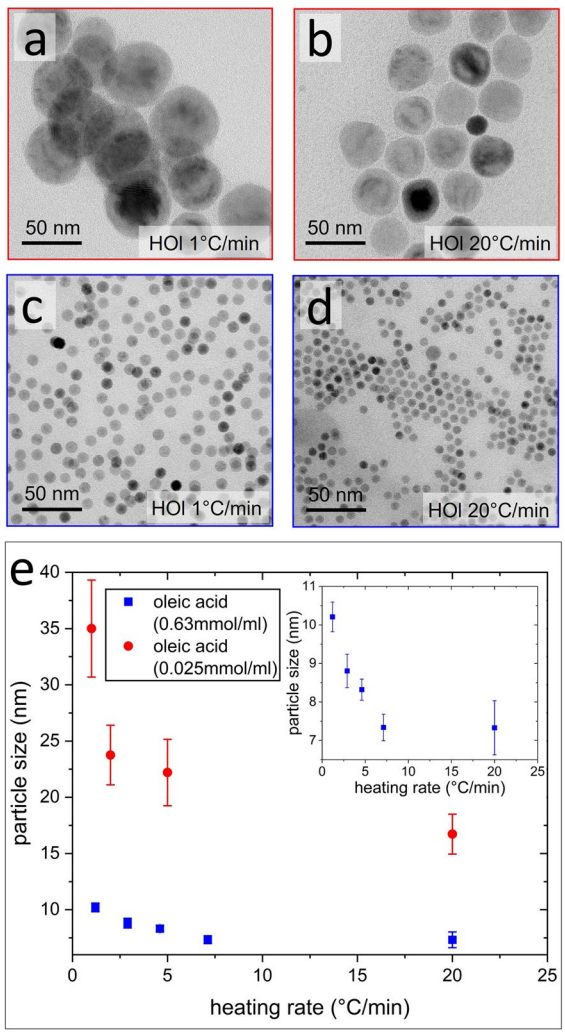

Fig. 3 TEM images of particles prepared with HOl as surfactant using different concentrations of (**a**, **b**) 0.025 mmol/ml and (**c**, **d**) 0.63 mmol/ml at different heating rates. (**e**) Corresponding averaged particle size as a function of heating rate. The inset shows an enlargement of the graph for the high amount of HOl case

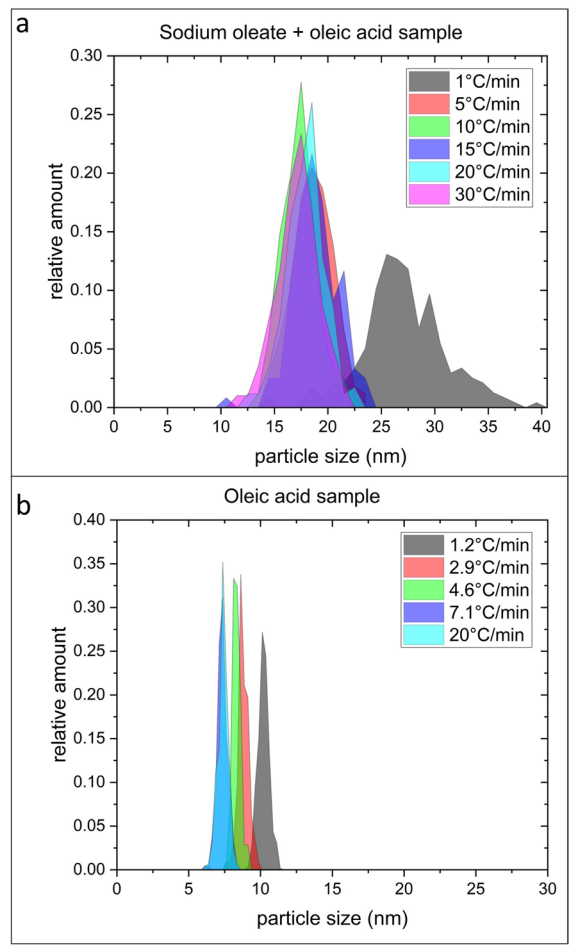

Fig. 4 Size distribution for particles (**a**) prepared with NaOl/HOl mixture and (**b**) with HOl (0.63 mmol/ml) as surfactant

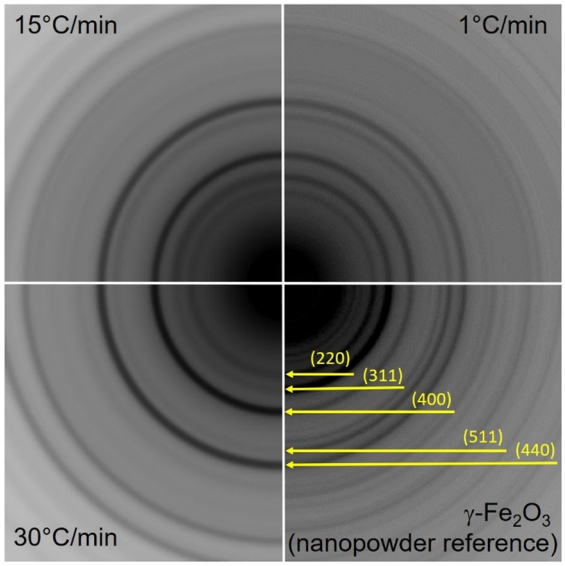

Fig. 5 Electron diffraction pattern of the cubic particles prepared with NaOl/HOl surfactant at different heating rates

the nanoparticles are monodispersed with a standard deviation of below 5% (Fig. 4b). Overall, for the higher heating rates (5, 10, 15, 20, and 30 °C/min), the size distribution remains more or less unchanged but shows a narrower distribution compared to the lowest heating rate (1 °C/min).

To reveal the structure of the nanoparticles, electron diffraction measurements were performed. Typical electron diffraction patterns of the various samples are shown in Fig. 5. For better comparison, the patterns were rotational averaged [26], i.e. the intensity from the centre of the diffractogram to its edges was averaged along the radius to get smooth diffraction rings instead of discrete spots. All patterns match very well with the γ-Fe_2O_3 reference pattern (Maghemite powder, Alfa Aesar GmbH Co KG). Please note that due to the preferred orientation of the cubic nanoparticles on the substrate, the intensities of the [220], [400], and [440] rings are higher compared to the γ-Fe_2O_3 reference pattern. Further, there is no evidence of the presence of α-Fe_2O_3. However, due to the similarity of the structures of γ-Fe_2O_3 and Fe_3O_4, and the line broadening due to the nanocrystalline nature of the sample, it is impossible to distinguish between these phases by electron diffraction.

As can be observed in Fig. 2c and e, some of the nanoparticles reveal a core–shell structure. An EELS analysis of a cubic nanoparticle prepared with NaOl/HOl at 30 °C/min heating rate is presented in Fig. 6a. The position of the Fe L_3 peak is an indicator for its oxidation state [27]. A higher oxidation state leads to a shift of the peak to higher energies, which is clearly seen in the linescan analysis presented in Fig. 6b when moving from the centre to the edges of the nanoparticle. From this, it can be concluded that the core of this nanoparticle contains some Fe^{2+} in the wustite phase ($Fe_{1-x}O$), while the iron in the shell is oxidized to Fe^{3+}. This is due to the fact that during the decomposition reaction, reducing agents like H_2 and CO may be formed that reduce the Fe^{3+} [28, 29]. In addition, no systematic influence of the heating rate on this core–shell structure was found. Please

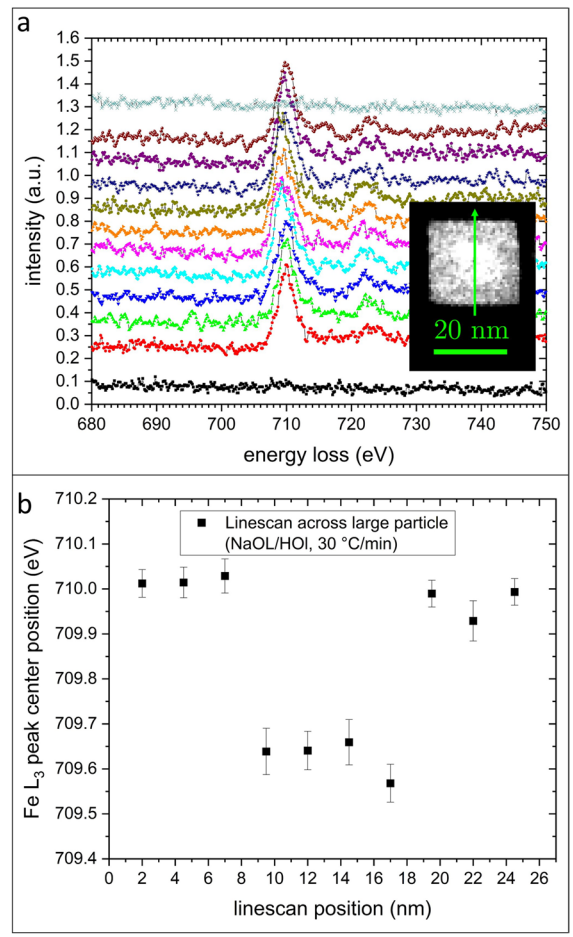

Fig. 6 (**a**) EEL spectra (around the Fe L_3 edge) taken at different locations across a cubic nanoparticle prepared with NaOl/HOl surfactant at 30 °C/min heating rate. The inset shows the corresponding scanning TEM image, which reveals a core–shell structure. (**b**) Variation of the Fe L_3 peak position across the core–shell nanoparticle presented in (**a**)

note that the wustite phase could not be detected in the electron diffractograms. However, this core–shell structure has been confirmed and discussed in great detail earlier [28, 30].

Discussion

The influence of the heating rate on the particle size is expected due to the model of LaMer [20]. Based on this model, the synthesis of the particles is divided into two parts: first, when the monomer concentration exceeds the critical supersaturation level due to the decomposition of the precursor while heating up the reactants, seed particles are formed. Second, these seed particles are growing until all of the precursor is consumed. This is schematically illustrated in Fig. 7. For different heating rates, the critical supersaturation level is reached after different times. During the growth phase the monomer concentration is below the supersaturation level, so no more seeds are formed, resulting in monodisperse particles. It is crucial to separate the seed formation and growth process; otherwise, polydisperse particles will be formed. According to T. Sugimoto [31], the nucleation rate depends strongly on the monomer concentration, whereas the growth rate only gradually increases with monomer concentration. In case of exceeding the critical supersaturation level, the number of formed nuclei is therefore very sensitive to the maximum monomer concentration reached in the solution and the time this state lasts. During nuclei formation, the monomers are consumed and the concentration drops down below the critical supersaturation level, inducing the growth phase. In case of a high heating rate, a strong overshooting in the supersaturation region is expected and therefore a high number of nuclei will form (Fig. 7I). Contrary, at a low heating rate, the monomer concentration just touches the supersaturation level, resulting in a low number of nuclei (Fig. 7III). In case of the same amount of precursor and under the assumption of an almost full consumption of this precursor, the final particle size should depend only on the number of particles formed.

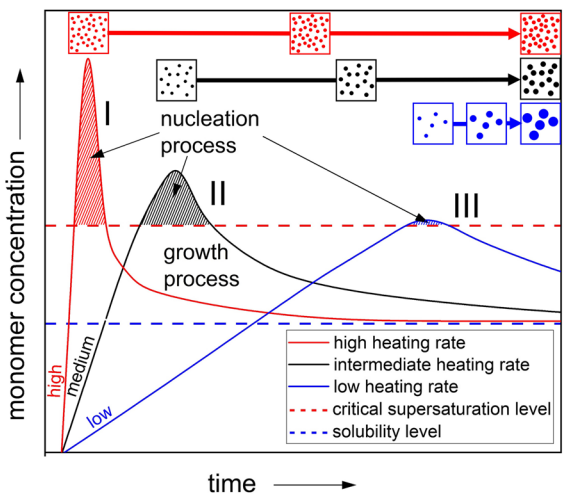

Fig. 7 Sketch of the nucleation and growth processes during particle synthesis for different heating rates (I–III) based on the LaMer model [20]

In our experiments with OHI as surfactant, a more continuous increase of the particle size was observed with lower heating rates (Fig. 3e), while with NaOl/HOl, only a significant increase for the lowest heating rate of 1 °C/min was found (Fig. 2g). For all of the higher heating rates, the particle size stays more or less constant, i.e. the number of nuclei does not increase further. Finally, the sizes of particles prepared without surfactant, shown in Fig. 2g, are slightly smaller than the particles with surfactants. This is in accordance with the literature [16] and can be explained by the stabilizing properties of the surfactants on the precursor. This lowers the nucleation rate and therefore leads to a lower number of particles, which results in larger particles.

Based on the LaMer model, the underlying mechanism that is responsible the particle size evolution will be discussed in the following.

To be consistent with our findings, at higher heating rates, the number of nuclei must become constant, i.e. independent of the heating rate. It is assumed that this is the case when all of the precursor is decomposed in the nucleation state (i.e. before the particle growth starts), with small nascent nuclei below their critical size to grow. This metastable state leads to the growth of some of the nuclei, reaching the critical size to be stable, whereas others dissolve again. Since the monomer concentration is limited by the amount of precursor, the system runs into this limit for high heating rates. For the growth phase, there is no precursor left. Following this argumentation, it should be possible to manipulate the particle size by changing the precursor concentration. In this case, a

higher precursor concentration should lead to larger particles. This was indeed confirmed by a further experiment where only the precursor concentration was varied from 100 to 1300 mg (dissolved in 10 ml of 1-octadecene). As shown in Fig. 8, a clear increase of particle size is visible with increasing precursor concentration. Similar results were also reported for a different precursor of manganese oleate in Ref. [32].

This conclusion is further supported by a study presented by Demortière et al. [33]. They used solvents with a boiling point (bp) close to the decomposition temperature (di-n-hexyl ether, bp 228 °C), and solvents with significantly higher boiling points (amongst others, di-n-octyl ether, bp 287 °C, octadecene, bp 317 °C, eicosene, bp 330 °C), applying a heating rate of 5 °C/min. They argue that the nucleation is more sensitive to temperature variations than the growth. When using a solvent with a boiling temperature close to the nucleation temperature, the nucleation is favoured and small particles are generated since the growth activation is low.

A similar behaviour was reported by Guardia et al. [21] for a slightly modified synthesis route using iron acetylacetonate with decanoic acid as stabilizer in dibenzyl ether. The size of the iron oxide nanoparticles could be tuned from 13 up to 180 nm by varying the heating rate from 5.2 down to 0.8 °C/min, respectively. Interestingly, they observed for the larger particles a significant increase of the size distribution.

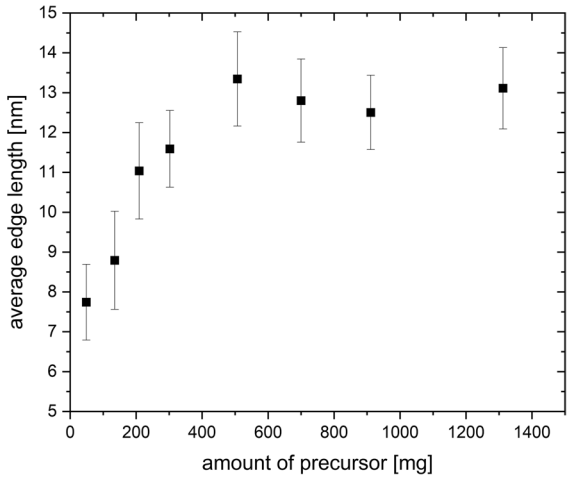

Fig. 8 Particle size as a function of the amount of precursor (heating rate: 20 °C/min, no surfactant used, constant amount of solvent)

This is explained by the fact that the nucleation step is more pronounced at higher heating rates, leading to a better separation of nucleation and growth. Besides experimental results, Sharifi Deshari et al. [22] conducted theoretical investigations on the influence of the heating rate on the growth of iron oxide nanoparticles by thermal decomposition of a precursor. By theoretical simulation based on precursor-to-monomer conversion, followed by nucleation and growth, they proved that for lower heating rates, larger particles are expected. This was confirmed by experiments based on the decomposition of iron acetylacetonate as precursor, resulting in particle sizes ranging from 6.3 up to 27 nm by varying the heating rate from 6.4 to 0.8 °C/min, respectively. They found also a saturation behaviour of the size with increasing heating rate. The behaviour was explained by the interplay between monomer formation and their consumption by nucleation and growth, arguing that at higher heating rates, a higher number of nuclei is formed and hence, the particles are smaller. This result matches well with the observation of this study and our qualitative explanation based on the LaMer model.

Stepanov et al. [23] observed as well an increased particle size for lower heating rates for the decomposition of iron oleate in 1-octadecane, using a different heating setup based on Wood's alloy. In particular, the particle size increased from 7 to 12 nm when the heating rate was decreased from 3.35 to 3.08 °C/min, respectively.

Z. Chen [34] observed also an increase in particle size when prepared at a lower heating rate but argues in a different way, where the higher heating rate favours the formation of slightly larger nuclei, leading to larger particles. However, there is no discussion about the number of particles or the amount of precursor together with the heating rate. For higher heating rates, the observed size broadening is explained by overlapping of the growth and nucleation processes. At a heating rate higher than 20 °C/min, no particles can be obtained because of incomplete nucleation and subsequent growth failure. In contrast, in our experiments, we observe particles even at heating rates above 30 °C/min. Furthermore, according to [34], by increasing the HOl concentration, the particle size should increase. But our results show the opposite effect (Fig. 3). It is assumed that the reason is the stabilizing role of the HOI surfactant on the precursor against decomposition. The

surfactant shifts the reaction equilibrium to the side of the educts at the beginning of the heating process. This leads to a raised decomposition temperature for a higher HOI concentration, and therefore, the nucleation rate is also increased. This results in a higher number of seed crystals and therefore leads to smaller particles.

In contrast, Yin et al. [35] report on a different behaviour. They synthesized iron oxide nanoparticles by thermal decomposition of iron pentacarbonyl. Varying the heating rate from 5 up to 35 °C/min did not show any influence on the particle size. However, the size distribution changed from 12 to 3% for the highest heating rate. It was concluded that a higher heating rate leads to a more homogeneous nucleation because the nucleation is finished within a shorter time interval. In our experiments, we have not observed a significant decrease of the size distribution with higher heating rate, as can be seen in Fig. 4.

Conclusion

The method to prepare nanoparticles by thermal decomposition of precursors offers many variables that influence the final particle morphology. Here, the influence of the employed surfactant (oleic acid and sodium oleate) and heating rate during the heating up process of the reaction solution on the particle size was investigated. By varying the heating rate from 1 up to 30 °C/min, a strong change of the particle size has been observed. The largest particles were obtained at the lowest heating rate while at high heating rates the size of the nanoparticles stays more or less the same. For the latter, the reason is probably a depletion of precursor in the nucleation phase. The evolution of the particle size with heating rate can be qualitatively understood in the frame of the LaMer model considering the nucleation and growth process.

Most of the prepared particles show a characteristic core–shell structure and their shape depends strongly on the used surfactant. The dominant structure is the cubic spinel structure of maghemite or magnetite, while in the core region of the particles, wustite is present.

The obtained results demonstrate the possibility for particle size and shape tuning by controlled thermal decomposition of metal organic complex precursors in the presence of surfactants. In combination with other techniques like solvents with higher boiling point [33, 36], the technique of lowering the heating rate could open the door to even larger, monodisperse particles.

Acknowledgements We thank R. Tidecks (University of Augsburg) for the stimulating discussions.

Author contribution Conceived and designed experiments: AU. Preparation of nanoparticle samples: MR, AU, AA, MK. TEM images and analysis: AU. Data evaluation and visualization: AU. Writing of manuscript and discussion of results: AU, MA.

Funding Open Access funding enabled and organized by Projekt DEAL.

Data availability The data generated during and/or analysed in the current study are available from the corresponding author on reasonable request.

Declarations

Competing interests The authors declare no competing interests.

References

1. Haun JB, Yoon TJ, Lee H, Weissleder R (2010) Magnetic nanoparticle biosensors. WIREs Nanomed Nanobiotechnol 2:291–304. https://doi.org/10.1002/wnan.84
2. Jiang C, Ng SM, Leung CW, Pong PWT (2017) Magnetically assembled iron oxide nanoparticle coatings and their integration with pseudo-spin-valve thin films. J Mater Chem C 5:252–262. https://doi.org/10.1039/C6TC03918A
3. Beygzadeh M, Alizadeh A, Khodaei MM, Kordestani D (2013) Biguanide/Pd$(OAc)_2$ immobilized on magnetic nanoparticle as a recyclable catalyst for the heterogeneous Suzuki reaction in aqueous media. Catal Commun 32:86–91. https://doi.org/10.1016/j.catcom.2012.11.028

4. Barati MR, Suzuki K, Selomulya C, Garitaonandia, JS. (2013) New T_c-tuned manganese ferrite-based magnetic implant for hyperthermia therapy application. IEEE Trans Magn 49:3460–3463. https://doi.org/10.1109/TMAG.2013.2246860
5. Wang YX (2011) Superparamagnetic iron oxide based MRI contrast agents: current status of clinical application. Quant Imaging Med Surg 1:35–40 https://doi.org/10.3978/j.issn.2223-4292.2011.08.03
6. Wang YX, Hussain SM, Krestin GP (2001) Superparamagnetic iron oxide contrast agents: physicochemical characteristics and applications in MR imaging. Eur Radiol 11(11):2319–2331. https://doi.org/10.1007/s003300100908
7. Halupka-Bryl M, Bednarowicz M, Dobosz B, Krzyminiewski R, Zalewski T, Wereszczynska B, Nowaczyk G, Jarek M, Nagasaki Y (2015) Doxorubicin loaded PEG-b-poly(4-vinylbenzylphosphonate) coated magnetic iron oxide nanoparticles for targeted drug delivery. J Magn Magn Mater 384:320–327. https://doi.org/10.1016/j.jmmm.2015.02.078
8. Kim DH, Nikles DE, Brazel CS (2010) Synthesis and characterization of multifunctional chitosan-$MnFe_2O_4$ nanoparticles for magnetic hyperthermia and drug delivery. Materials 3(7):4051–4065. https://doi.org/10.3390/ma3074051
9. Pankhurst QA, Connolly J, Jones SK, Dobson J (2003) Applications of magnetic nanoparticles in biomedicine. J Phys D Appl Phys 36(13):R167-R181 https://doi.org/10.1088/0022-3727/36/13/201
10. Qiang Y, Antony J, Sharma A, Nutting J, Sikes D, Meyer D (2006) Iron/iron oxide core-shell nanoclusters for biomedical applications. J Nanopart Res 8:489–496. https://doi.org/10.1007/s11051-005-9011-3
11. Wu R, Qu J (2009) Removal of water soluble azo dyes by magnetic material $MnFe^2O^4$. J Chem Technol Biotechnol 80:20–27 https://doi.org/10.1002/jctb.1142
12. Lv S, Chen X, Ye Y, Yin S, Cheng J, Xia M (2009) Rice hull/$MnFe^2O^4$ composite: preparation, characterization and its rapid microwave-assisted COD removal for organic wastewater. J Hazard Mater 171:634–639. https://doi.org/10.1016/j.jhazmat.2009.06.039
13. John M, Heuss-Aßbichler S, Tandon K, Ullrich A (2019) Recovery of Ag and Au from synthetic and industrial wastewater by 2-step ferritization and Lt-delafossite process via precipitation. J Water Process Eng 30:100532. https://doi.org/10.1016/j.jwpe.2017.12.001
14. Park J, An K, Hwang Y, Park JG, Noh HJ, Kim JY, Park JH, Hwang NM, Hyeon T (2004) Ultra-large-scale syntheses of monodisperse nanocrystals. Nat Mater 3:891–895 https://doi.org/10.1038/nmat1251
15. Hyeon T, Lee SS, Park J, Chung Y, Na HB (2001) Synthesis of highly crystalline and monodisperse maghemite nanocrystallites without a size-selection process. J Am Chem Soc 123(51):12798–12801. https://doi.org/10.1021/ja016812s
16. Hai HT, Yang HT, Kura H, Hasegawa D, Ogata Y, Takahashi M, Ogawa T (2010) Size control and characterization of wustite (core)/spinel (shell) nanotubes obtained by decomposition of iron oleate complex. J Colloid Interface Sci 346:37–42. https://doi.org/10.1016/j.jcis.2010.02.025
17. Kovalenko MV, Bodnarchuk MI, Lechner RT, Hesser G, Schaeffler F, Heiss W (2007) Fatty acid salts as stabilizers in size- and shape-controlled nanocrystal synthesis: the case of inverse spinel iron oxide. J Am Chem Soc 129(20):6352–6353. https://doi.org/10.1021/ja0692478
18. Sun S, Zeng H (2002) Size-controlled synthesis of magnetite nanocrystals. J Am Chem Soc 124:8204–8205. https://doi.org/10.1021/ja026501x
19. Tong S, Quinto ChA, Zhang L, Mohindra P, Bao G (2017) Size-dependent heating of magnetic iron oxide nanoparticles. ACS Nano 11:6808–6816. https://doi.org/10.1021/acsnano.7b01762
20. LaMer VK, Dinegar RH (1950) Theory, production and mechanism of formation of monodispersed hydrosols. J Am Chem Soc 72(11):4847–4854. https://doi.org/10.1021/ja01167a001
21. Guardia P, Pérez-Juste J, Labarta I, Batlle X, Liz-Marzán LM (2010) Heating rate influence on the synthesis of iron oxide nanoparticles: the case of decanoic acid. Chem Commun 46:6108–6110. https://doi.org/10.1039/c0cc01179g
22. Sharifi Dehsari H, Heidari M, HaldaRibeiro A, Tremel W, Jakob G, Donadio D, Potestio R, Asadi K (2017) Combined experimental and theoretical investigation of heating rate on growth of iron oxide nanoparticles. Chem Mater 29(22):9648–9656. https://doi.org/10.1021/acs.chemmater.7b02872
23. Stepanov A, Mustafina A, Mendes RG, Rümmeli MH, Gemming T, Popova E, Nizameev I, Kadirov M (2016) Impact of heating mode in synthesis of monodisperse iron-ocide nanoparticles via oleate decomposition. J Iran Chem Soc 13(2):299–305. https://doi.org/10.1007/s13738-015-0737-2
24. Herrera AP, Polo-Corrales L, Chavez E, Cabarcas-Bolivar J, Uwakweh ONC, Rinaldi C (2013) Influence of ageing time of oleate precursor on the magnetic relaxation of cobalt ferrite nanoparticles synthesized by the thermal deconposition method. J Magn Magn Mater 328:41–52. https://doi.org/10.1016/j.jmmm.2012.09.069
25. Ristroph KD, Prud'homme RK (2019) Hydrophobic ion pairing: encapsulating small molecules, peptides, and proteins into nanocarriers. Nanoscale Adv 1(11):4207-4237. https://doi.org/10.1039/C9NA00308H. See also: Database., N. C. f. B. I. P. Sodium oleate, CID=23665730. https://pubchem.ncbi.nlm.nih.gov/compound/23665730 and Database., N. C. f. B. I. P. Oleic acid, CID=445639. https://pubchem.ncbi.nlm.nih.gov/compound/445639
26. Mitchell DRG (2008) DiffTools: electron diffraction software tools for DigitalMicrograph™. Microsc Res Tech 71:588–593. https://doi.org/10.1002/jemt.20591
27. Tan H, Verbeeck J, Abakumov A, Tendeloo GV (2012) Oxidation state and chemical shift investigation in transition metal oxides by EELS. Ultramicroscopy 116:24–33. https://doi.org/10.1016/j.ultramic.2012.03.002
28. Chen C-J, Chiang R-K, Lai H, Lin C-R (2010) Characterization of monodisperse Wüstite nanoparticles following partial oxidation. J Phys Chem C 114:4258–4263. https://doi.org/10.1021/jp908153y
29. Kim D, Park J, An K, Yang N-K, Park J-G, Hyeon T (2007) Synthesis of hollow iron nanoframes. J Am Chem Soc 129:5812–5813. https://doi.org/10.1021/ja070667m
30. Ullrich A, Rahman MM, Longo P, Horn S (2019) Synthesis and high-resolution structural and chemical analysis of iron-manganese-oxide core-shell nanocubes. Sci Rep 9:19264. https://doi.org/10.1038/s41598-019-55397-z
31. Sugimoto T (2019) Monodispersed particles. Elsevier, Amsterdam, Oxford

32. Ullrich A (2013) Präparation von Eisenoxid-, Manganoxid- und Kompositnanopartikeln und deren mikroskopische Charakterisierung. Dissertation, University of Augsburg. Mensch und Buch Verlag, Berlin
33. Demotiére A, Panissod P, Pichon BP, Pourroy G, Guillon D, Donnio B, Bégin-Colin S (2011) Size-dependent properties of magnetic iron oxide nanocrystals. Nanoscale 3:225–232. https://doi.org/10.1039/c0nr00521e
34. Chen Z (2012) Size and shape controllable synthesis of monodisperse iron oxide nanoparticles by thermal decomposition of iron oleate complex. Synth React Inorg, Met-Org, Nano-Met Chem 42:1040–1046. https://doi.org/10.1080/15533174.2012.680126
35. Yin M, Willis A, Redl F, Turro NJ, O'Brien SP (2004) Influence of capping groups on the synthesis of γ-Fe_2O_3 nanocrystals. J Mater Res 19:1208–1215. https://doi.org/10.1557/JMR.2004.0157
36. Wetterskog E, Agthe M, Mayence A, Grins J, Wang D, Rana S, Ahniyaz A, Salazar-Alvarez G, Bergström L (2014) Precise control over shape and size of iron oxide nanocrystals suitable for assembly into ordered particle arrays. Sci Technol Adv Mater 15:055010. https://doi.org/10.1088/1468-6996/15/5/055010